

Shear and Bulk Acceleration Viscosities in Simple Fluids

Johannes Renner¹, Matthias Schmidt¹, and Daniel de las Heras^{1*}

Theoretische Physik II, Physikalisches Institut, Universität Bayreuth, D-95440 Bayreuth, Germany

 (Received 30 October 2021; accepted 9 February 2022; published 4 March 2022)

Inhomogeneities in the velocity field of a moving fluid are dampened by the inherent viscous behavior of the system. Both bulk and shear effects, related to the divergence and the curl of the velocity field, are relevant. On molecular time scales, beyond the Navier-Stokes description, memory plays an important role. Using molecular and overdamped Brownian dynamics many-body simulations, we demonstrate that analogous viscous effects act on the acceleration field. This acceleration viscous behavior is associated with the divergence and the curl of the acceleration field, and it can be quantitatively described using simple exponentially decaying memory kernels. The simultaneous use of velocity and acceleration fields enables the description of fast dynamics on molecular scales.

DOI: 10.1103/PhysRevLett.128.094502

The viscous force determines the resistance of a moving fluid to change the magnitude and the direction of the flow. Such a viscous response, originated by the interparticle interactions, is relevant in, e.g., lubrication [1], protein dynamics in biological solvents [2,3], viscotaxis [4,5], magnetic [6] and quantum [7] fluids, lava flows [8], cardiovascular events [9,10], food manufacturing [11], and cosmological models [12,13]. Viscous effects are associated with inhomogeneities in the velocity field of the fluid. The viscous force $\mathbf{f}_{\text{vis}}(\mathbf{r}, t)$ experienced by a particle of a fluid at position \mathbf{r} and time t contains bulk $\mathbf{f}_b(\mathbf{r}, t)$ and shear $\mathbf{f}_s(\mathbf{r}, t)$ contributions, i.e., $\mathbf{f}_{\text{vis}} = \mathbf{f}_b + \mathbf{f}_s$. These contributions are associated with the divergence $\nabla \cdot \mathbf{v}$ (bulk) and the curl $\nabla \times \mathbf{v}$ (shear) of the velocity field $\mathbf{v}(\mathbf{r}, t)$, respectively. Specifically, \mathbf{f}_{vis} in the Navier-Stokes [14] equations is

$$\rho \mathbf{f}_{\text{vis}} = \eta_b \nabla \nabla \cdot \mathbf{v} - \eta_s \nabla \times (\nabla \times \mathbf{v}), \quad (1)$$

where $\rho(\mathbf{r}, t)$ is the density profile and η_α with $\alpha = b, s$ are transport coefficients known as bulk and shear viscosities.

Here, we demonstrate the occurrence in simple fluids of analog viscous contributions, but generated by the divergence and the curl of the acceleration field $\mathbf{a}(\mathbf{r}, t)$. We use custom flow [15,16] to design specific flows (driven by external forces) in which we can unambiguously single out the acceleration contribution of the viscous force. We consider inhomogeneous and rapidly changing flows. Hence, memory effects and inhomogeneities of the density profile cannot be ignored and need to be included in Eq. (1). We propose the following expressions for bulk and shear viscous forces of an inhomogeneous simple fluid,

$$\mathbf{f}_b(\mathbf{r}, t) = \frac{1}{\rho} \int_0^t dt' [K_b^v(t-t') \nabla (\rho \rho' \nabla \cdot \mathbf{v}') + K_b^a(t-t') \nabla (\rho \rho' \nabla \cdot \mathbf{a}')], \quad (2)$$

$$\mathbf{f}_s(\mathbf{r}, t) = \frac{-1}{\rho} \int_0^t dt' [K_s^v(t-t') \nabla \times (\rho \rho' \nabla \times \mathbf{v}') + K_s^a(t-t') \nabla \times (\rho \rho' \nabla \times \mathbf{a}')], \quad (3)$$

where we leave out the dependence on \mathbf{r} and t , primed quantities are evaluated at t' , e.g., $\rho' = \rho(\mathbf{r}, t')$, and K_α^Γ (with $\alpha = b, s$ and $\Gamma = \mathbf{v}, \mathbf{a}$) are exponentially decaying memory kernels

$$K_\alpha^\Gamma(t-t') = \frac{c_\alpha^\Gamma}{\tau_\alpha^\Gamma} e^{-(t-t')/\tau_\alpha^\Gamma}, \quad (4)$$

with constant amplitudes c_α^Γ and memory times τ_α^Γ . The first terms of Eqs. (2) and (3) are the familiar bulk and shear viscous forces in the Navier-Stokes equations, Eq. (1), for flows with inhomogeneous density profiles and with the addition of a memory kernel. The second terms have identical structure but replacing \mathbf{v} by \mathbf{a} and represent therefore a viscous response generated by an inhomogeneous acceleration field. The viscous force in Eq. (1) with viscosities $\eta_\alpha = c_\alpha^v \rho^2$ follows from the velocity contributions of Eqs. (2) and (3) by ignoring the effect of both memory and an inhomogeneous density profile. Our specific form for \mathbf{f}_{vis} arises in power functional theory [17–19] by retrieving the first terms of an expansion in acceleration gradients; see additional details in the Supplemental Material [20].

To demonstrate the occurrence of viscous effects associated with the acceleration field, we need to disentangle the velocity and the acceleration contributions from the total viscous force. This requires a complete control over the characteristics of the flow, which we achieve using custom flow [15,16]. Custom flow uses particle-based simulations to find numerically the spatially and temporally resolved external field required to generate the desired

dynamics of a many-body system. The one-body density $\rho(\mathbf{r}, t)$ and current $\mathbf{J}(\mathbf{r}, t) = \rho(\mathbf{r}, t)\mathbf{v}(\mathbf{r}, t)$ profiles serve as input target fields, while the external field $\mathbf{f}_{\text{ext}}(\mathbf{r}, t)$ that generates these targets is the output of the method. At each time, $\mathbf{f}_{\text{ext}}(\mathbf{r}, t)$ is constructed iteratively. At iteration $k + 1$ we add to the external force of the previous iteration k a term proportional to the difference between the target (\mathbf{J}) and sampled ($\mathbf{J}^{(k)}$) currents, i.e., $\mathbf{f}_{\text{ext}}^{(k+1)} = \mathbf{f}_{\text{ext}}^{(k)} + \alpha_0(\mathbf{J} - \mathbf{J}^{(k)})$. Here, the parameter $\alpha_0(\mathbf{r}, t) > 0$ is chosen to ensure that the difference between the target and sampled current fields progressively shrinks. Details about custom flow are provided in Refs. [15,16] and in the Supplemental Material [20]. Custom flow is essential here to tailor the dynamics of the system such that the viscous force can be (i) easily measured and (ii) unambiguously split into velocity and acceleration contributions. We use molecular dynamics (MD) simulations to study a three-dimensional system of particles of mass m interacting via the short-ranged and purely repulsive Weeks-Chandler-Andersen pair potential [21] with length and energy parameters σ

and ϵ , respectively. We work in units of σ , ϵ , and m . Hence, the unit of time is $\tau = \sqrt{m\sigma^2/\epsilon}$. We consider two different flows that represent pure bulk (compressible) and shear situations. In both flows the one-body current \mathbf{J} factorizes into a (vectorial) spatial part $\mathbf{J}_{\mathbf{r}}$ and a (scalar) temporal part J_t , i.e., $\mathbf{J}(\mathbf{r}, t) = J_t(t)\mathbf{J}_{\mathbf{r}}(\mathbf{r})$.

The temporal part is common to both flows; see Fig. 1(a) and the Supplemental Material [20] for the mathematical expression. The current increases from the initial time until $t_{\uparrow} = 1\tau$, then remains constant (quasisteady state) until $t_c = 5\tau$, decreases until it vanishes at $t_{\downarrow} = 6\tau$, and it stays zero afterward. This setup helps to disentangle the velocity and the acceleration contributions from \mathbf{f}_{vis} since \mathbf{v} and \mathbf{a} are parallel to each other during the increase of \mathbf{J} , but they are antiparallel during the decrease of \mathbf{J} . Both \mathbf{v} and \mathbf{a} stay unchanged during the quasisteady state and during the final evolution toward equilibrium which is useful to characterize memory effects.

Both flows are designed to have a stationary one-body density during the whole time evolution, i.e., $\dot{\rho}(\mathbf{r}, t) = 0$,

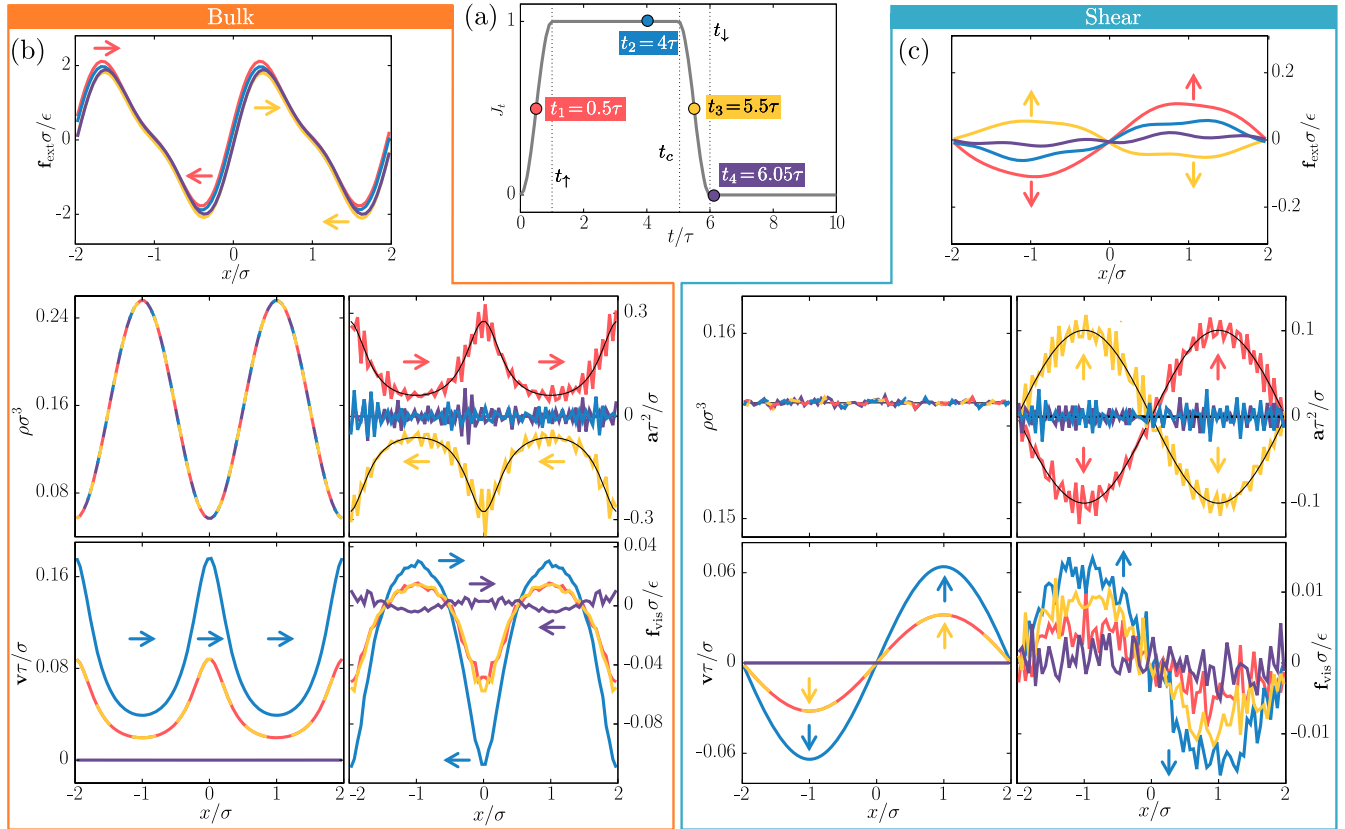


FIG. 1. (a) Temporal part of the current J_t vs time t common to the bulk (b) and shear (c) flows. Four times t_i with $i = 1, 2, 3$, and 4 are highlighted with colored circles. The vertical dotted lines indicate the times t_{\uparrow} , t_c , and t_{\downarrow} . (b),(c) The external force \mathbf{f}_{ext} , density ρ , velocity \mathbf{v} , acceleration \mathbf{a} , and viscous force \mathbf{f}_{vis} profiles as a function of x for the bulk and shear flows, respectively. To improve the visualization, the external force has been smoothed by eliminating high-frequency Fourier modes (see details and raw data in the Supplemental Material [20]). The thin black solid lines are the target fields that coincide (up to numerical accuracy) with the sampled fields. The color of the profiles indicates the time $t_1 = 0.5\tau$ (red), $t_2 = 4\tau$ (blue), $t_3 = 5.5\tau$ (yellow), and $t_4 = 6.05\tau$ (purple), as indicated in (a). The arrows indicate the direction of the vector field at specific locations (arrow position) and times (arrow color).

where the overdot denotes a time derivative. This simplifies the data analysis since as a direct consequence the viscous forces in Eqs. (2) and (3) also factorize into spatial and temporal terms [20]

$$\mathbf{f}_\alpha(\mathbf{r}, t) = C_\alpha(t)\mathbf{f}_{r,\alpha}(\mathbf{r}), \quad \alpha = b, s. \quad (5)$$

Bulk flow.—Here, by construction $\nabla \times \mathbf{v} = 0$ and $\nabla \times \mathbf{a} = 0$ but $\nabla \cdot \mathbf{v} \neq 0$ and $\nabla \cdot \mathbf{a} \neq 0$. Hence, only bulk effects contribute to the viscous force, i.e., $\mathbf{f}_{\text{vis}} = \mathbf{f}_b$. We take the one-body density to be inhomogeneous, but only along the x direction. The one-body current has only an x component which is taken to be constant in space:

$$\rho(\mathbf{r}, t) = \rho(x) = \rho_0 - \rho_1 \cos(4\pi x/L_x), \quad (6)$$

$$\mathbf{J}(\mathbf{r}, t) = \mathbf{J}(t) = J_0 J_t(t) \hat{\mathbf{e}}_x, \quad (7)$$

with average density $\rho_0 \sigma^3 = 0.15625$, amplitude $\rho_1 \sigma^3 = 0.1$, side length of the simulation box $L_x/\sigma = 4$, and maximum value of the current $J_0 \tau \sigma^2 = 0.01$. Both the velocity $\mathbf{v} = \mathbf{J}/\rho$ and the acceleration $\mathbf{a} = \dot{\mathbf{v}} = \dot{\mathbf{J}}/\rho$ (where the second equality holds here since $\dot{\rho} = 0$) are inhomogeneous in space even though the current is homogeneous.

The external force that produces this bulk flow together with density, velocity, and acceleration profiles sampled in MD are shown in Fig. 1(b) for four selected times. The viscous force \mathbf{f}_{vis} [also shown in Fig. 1(b)] is the part of the internal force that changes sign under flow reversal [20,22]. The four times selected in Fig. 1 represent the different regimes of the time evolution imposed by J_t ; see Fig. 1(a). At $t_1 = 0.5\tau$, i.e., $t_1 < t_\uparrow$, the current increases, and both \mathbf{v} and \mathbf{a} point in the same direction. At $t_2 = 4\tau$, i.e., $t_\uparrow < t_2 < t_c$, the system is in a quasisteady state with negligible memory effects (we know this by monitoring the viscous force which does not change with time). The acceleration vanishes everywhere, and the velocity profile remains unchanged in this time interval. At $t_3 = 5.5\tau$, i.e., $t_c < t_3 < t_\downarrow$ the current decreases. The velocity and the acceleration profiles have opposite sign everywhere. Finally, at $t_4 = 6.05\tau$, i.e., $t_4 > t_\downarrow$, both \mathbf{v} and \mathbf{a} vanish everywhere. However, due to memory effects the system has not reached equilibrium yet; there is, for example, a viscous force generated by the history of \mathbf{v} and \mathbf{a} .

A visual inspection of the viscous force \mathbf{f}_{vis} , in Fig. 1(b), reveals two strong indications that the acceleration profile contributes to the viscosity. First, at t_4 the viscous force points in the opposite direction than at the previous times. Hence, the history of the acceleration profile must be dominating the viscosity since the velocity profile does not change its sign during the whole time evolution. Only \mathbf{a} changes sign during the decrease of the current [compare the acceleration profiles at times t_1 and t_3 in Fig. 1(b)]. Second, the profiles \mathbf{f}_{vis} at times t_1 and t_3 are similar. At these two times the velocity profiles are identical by

construction; see Figs. 1(a) and 1(b). However, \mathbf{a} and the history of both \mathbf{v} and \mathbf{a} are different. Since the viscosity at a given time depends on the history of the system, the contribution to the viscosity due to the acceleration must be canceling the contribution due to the history of the velocity profile. Otherwise, the viscous force at these times would differ.

The temporal part $C_b(t)$ for the bulk flow [see Eq. (5)] can be understood as the variation of the strength of the viscous force over time. Results are shown in Fig. 2(a). Clearly, C_b achieves larger values than at the quasisteady state for times around t_\uparrow , and smaller (negative) values than in equilibrium ($C_b = 0$) for times around t_\downarrow . The acceleration is responsible for the overshoot and the undershoot around the times t_\uparrow and t_\downarrow because \mathbf{a} is the only field that flips its sign during the increase and during the decrease of the current. Note that if \mathbf{a} does not contribute to the bulk viscous force, then the negative values of C_b would indicate an unphysical negative viscosity.

We next compare the MD data to our expression for the viscous force \mathbf{f}_b , Eq. (2), to obtain the kernel parameters; see the Supplemental Material [20] for details.

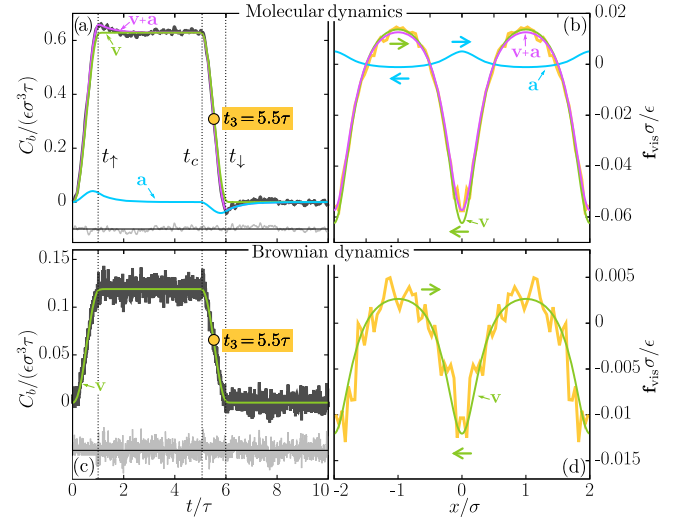


FIG. 2. (a) Temporal dependency of the bulk viscous force C_b as a function of time t in molecular dynamics simulations (thick black line) and theoretically (violet) for the bulk flow. The vertical dotted lines indicate the times t_\uparrow , t_c , and t_\downarrow . The time $t_3 = 5.5\tau$ is highlighted with a yellow circle. The light gray line fluctuating around the horizontal line is the difference between simulation (thick black) and theory (violet). (b) Bulk viscous force \mathbf{f}_{vis} as a function of x at time $t_3 = 5.5\tau$ according to MD (yellow) and theory (violet). The force points along the x axis. The colored arrows indicate the direction of the corresponding force at selected positions. The contributions of the velocity (green) and of the acceleration (blue) to the total signal (violet) are also shown in (a) and (b). The bottom panels (c) and (d) show the same data as the top panels, but using overdamped Brownian dynamics instead of MD. In BD only the velocity field contributes to the viscosity.

The amplitudes are $c_b^v/(\epsilon\sigma^3\tau) = 0.63$, $c_b^a/(\epsilon\sigma^3\tau^2) = 0.044$, and the memory times are $\tau_b^v/\tau = 0.043$, $\tau_b^a/\tau = 0.56$. The partial contributions of the velocity and the acceleration fields to C_b and \mathbf{f}_{vis} are shown in Figs. 2(a) and 2(b), respectively. The sum of both contributions agrees quantitatively with the MD data.

To assure that the overshoot and the undershoot in C_b are indeed due to the acceleration field, we performed overdamped Brownian dynamics (BD) simulations for exactly the same flow (using BD custom flow [15,20] and the usual assumption that the random force does not depend on the external force [23]). Since the system is overdamped, the acceleration does not play any role, and indeed, there is no overshoot or undershoot in C_b [Fig. 2(c)]. Both C_b and \mathbf{f}_{vis} are well reproduced theoretically using only the velocity field, Figs. 2(c) and 2(d), with kernel parameters $c_b^v/(\epsilon\sigma^3\tau) = 0.117$ and $\tau_b^v/\tau = 0.041$.

Shear flow.—We next consider a flow in which $\nabla \cdot \mathbf{v} = 0$ and $\nabla \cdot \mathbf{a} = 0$ but $\nabla \times \mathbf{v} \neq 0$ and $\nabla \times \mathbf{a} \neq 0$. Hence, only shear effects contribute to the viscous force, i.e., $\mathbf{f}_{\text{vis}} = \mathbf{f}_s$. Using custom flow we set the density profile to be homogeneous and the current to be a shear wave pointing in the y direction with modulation along the x direction,

$$\rho(\mathbf{r}, t) = \rho_0, \quad (8)$$

$$\mathbf{J}(\mathbf{r}, t) = \mathbf{J}(x, t) = J_0 \sin(2\pi x/L_x) J_t(t) \hat{\mathbf{e}}_y, \quad (9)$$

with $\rho_0\sigma^3 = 0.15625$, $L_x/\sigma = 4$, and $J_0\tau\sigma^2 = 0.01$.

Figure 1(c) shows the external force required to produce the flow along with results for ρ , \mathbf{v} , \mathbf{a} , and \mathbf{f}_{vis} at the same four different times as in the previous flow. A visual inspection of the data does not reveal the acceleration contribution since (i) for times $t_1 = 0.5\tau$ and $t_3 = 5.5\tau$ the curves are different (suggesting either a large memory time of the velocity contribution or a strong effect of the acceleration) and (ii) \mathbf{f}_{vis} does not flip the sign after the one-body current vanishes. Also, in contrast to the bulk flow, no apparent over- or undershoot is present in $C_s(t)$, i.e., the temporal part of \mathbf{f}_{vis} [see Fig. 3(a) and Eq. (5)]. For the shear flow we find that the amplitudes $c_s^v/(\epsilon\sigma^3\tau) = 0.56$ and $c_s^a/(\epsilon\sigma^3\tau^2) = 0.059$, and the memory times $\tau_s^v = 0.24\tau$, $\tau_s^a = 0.23\tau$ yield quantitative agreement between simulation data and our theory for both the temporal, Fig. 3(a), and the spatial dependence of \mathbf{f}_{vis} , Fig. 3(b). In contrast to the bulk flow, the memory times of \mathbf{a} and \mathbf{v} are now comparable, which partially hides the effect of the acceleration. To demonstrate the importance of \mathbf{a} we use only the velocity contribution and obtain $c_s^v/(\epsilon\sigma^3\tau) = 0.56$ and $\tau_s^v/\tau = 0.13$ as the optimal kernel parameters. The resulting curve for C_s [see Fig. 3(a)] deviates from the MD data around the times t_\uparrow (curve above MD data) and t_\downarrow (curve below MD data). This indicates that \mathbf{a} indeed contributes since its sign change around these times can correct these deviations.

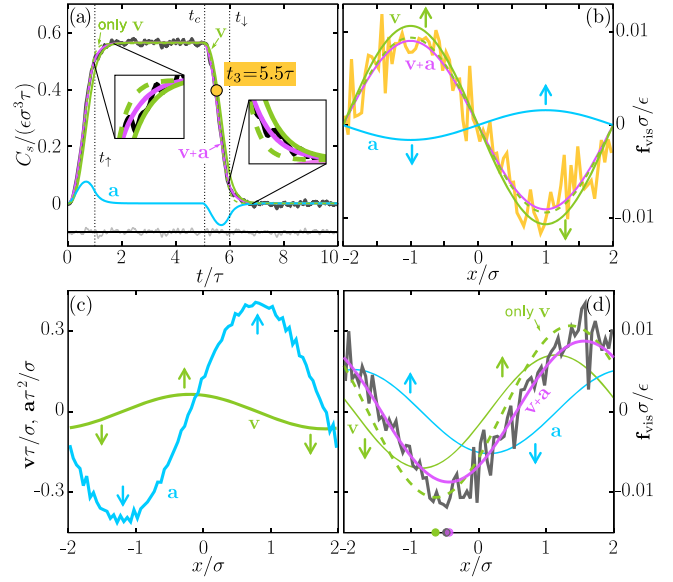


FIG. 3. (a) Temporal dependency of the shear viscous force C_s as a function of time t in MD simulations (thick black line) and theoretically (violet) for the shear flow. The light gray line fluctuating around the horizontal line is the difference between simulation (thick black) and theory (violet). (b) Shear viscous force \mathbf{f}_{vis} as a function of x at time $t_3 = 5.5\tau$ according to MD (yellow) and theory (violet). The force points along the y axis. (c) Illustrative velocity (green) and acceleration (blue) profiles vs x for the traveling shear wave ($t = 2.7\tau$). Note that \mathbf{a} and \mathbf{v} are not in phase. (d) Viscous force vs x for the traveling shear wave according to MD (thick black) and theory (violet) ($t = 2.7\tau$). The colored arrows indicate the direction of the corresponding field at the selected positions. The theoretical contributions of \mathbf{v} (green) and \mathbf{a} (blue) to the total signal (violet) are also shown in panels (a), (b), and (d) together with the theoretical predictions using only the velocity field (dashed green line). The colored circles over the x axis in (d) indicate the position of the minimum of \mathbf{f}_{vis} according to MD (gray), and theory using both contributions (violet) or only the velocity contribution (green).

To further ascertain the reality of the acceleration contribution, we use the obtained parameters for the amplitudes and the memory times to describe a variation of the flow. Instead of decreasing the one-body current after t_c , we keep the amplitude of the current unchanged and let the shear wave travel in the positive x direction. Specifically, after time $t = 2\tau > t_\uparrow$ we replace the x coordinate in Eq. (9) by $x - v_s t$ with constant velocity $v_s = 4\tau/\sigma$. Hence, the acceleration field is shifted by $\pi/2$ with respect to the velocity field; see Fig. 3(c). The phase difference between \mathbf{v} and \mathbf{a} has an effect on the viscous force; see Fig. 3(d). Using the kernel parameters for the previous flow and both the velocity and the acceleration contributions we reproduce the simulation data. In contrast, using the parameters obtained only with the velocity contribution results in a clear phase shift compared with the MD data. See the Supplemental Material [20] for more details.

Our results demonstrate the existence of shear and bulk acceleration viscous forces generated by inhomogeneities of the acceleration field. These forces act in addition to the usual viscous response associated with the velocity field. In our examples the contribution of the acceleration to the viscous force is quantitatively significant. Acceleration viscous forces might be also relevant in flows with rapid temporal changes of the velocity field such as in shock waves [24–28], turbulent flows [29–31] including atmospheric and oceanic flows [32], inertial microfluidics [33–35], the description of flows at the nanoscale [36–38], mudflows [39], single-bubble sonoluminescence [40,41], and viscous cosmological models [12,42].

We did not use a thermostat due to the low heat production in both flows (the temperature increase was less than 2% from the initial to the final state [20]). However, custom flow can be used with thermostats [16], and it would be interesting to compare the effect of the acceleration viscosities in thermalized and nonthermalized flows.

We use here a rather simple kernel as compared with other approaches [43–46]. The use of simple memory kernels that decay exponentially in time is only possible because we use all physically relevant variables, i.e., both \mathbf{v} and \mathbf{a} . Since \mathbf{a} and \mathbf{v} are related to each other, it should be possible to describe \mathbf{f}_{vis} using only \mathbf{v} or \mathbf{a} together with a complicated kernel. Such a kernel would be tailored to the specific flow instead of being general to every situation. For example, it might be possible to describe the viscous force of the bulk flow using only \mathbf{v} and a complex memory kernel with a negative tail.

This work is supported by the German Research Foundation (DFG) via Project No. 447925252.

*Corresponding author.

<https://www.danieldelasheras.com>
delasheras.daniel@gmail.com

- [1] B. Bhushan, J. N. Israelachvili, and U. Landman, Nanotribology: Friction, wear and lubrication at the atomic scale, *Nature (London)* **374**, 607 (1995).
- [2] A. Ansari, C. M. Jones, E. R. Henry, J. Hofrichter, and W. A. Eaton, The role of solvent viscosity in the dynamics of protein conformational changes, *Science* **256**, 1796 (1992).
- [3] B. Zagrovic and V. Pande, Solvent viscosity dependence of the folding rate of a small protein: Distributed computing study, *J. Comput. Chem.* **24**, 1432 (2003).
- [4] B. Liebchen, P. Monderkamp, B. ten Hagen, and H. Löwen, Viscotaxis: Microswimmer Navigation in Viscosity Gradients, *Phys. Rev. Lett.* **120**, 208002 (2018).
- [5] C. Datt and G. J. Elfring, Active Particles in Viscosity Gradients, *Phys. Rev. Lett.* **123**, 158006 (2019).
- [6] J.-C. Bacri, R. Perzynski, M. I. Shliomis, and G. I. Burde, Negative-viscosity Effect in a Magnetic Fluid, *Phys. Rev. Lett.* **75**, 2128 (1995).
- [7] J. E. Avron, R. Seiler, and P. G. Zograf, Viscosity of Quantum Hall Fluids, *Phys. Rev. Lett.* **75**, 697 (1995).
- [8] R. W. Griffiths, The dynamics of lava flows, *Annu. Rev. Fluid Mech.* **32**, 477 (2000).
- [9] G. D. O. Lowe, A. J. Lee, A. Rumley, J. F. Price, and F. G. R. Fowkes, Blood viscosity and risk of cardiovascular events: The Edinburgh Artery Study, *Br. J. Haematol.* **96**, 168 (1997).
- [10] H. C. Kwaan, The hyperviscosity syndromes, *Semin. Thromb. Hemostasis* **29**, 433 (2003).
- [11] G. Tabilo-Munizaga and G. V. Barbosa-Cnovas, Rheology for the food industry, *J. Food Eng.* **67**, 147 (2005).
- [12] R. Maartens, Dissipative cosmology, *Classical Quantum Gravity* **12**, 1455 (1995).
- [13] J.-S. Gagnon and J. Lesgourgues, Dark goo: Bulk viscosity as an alternative to dark energy, *J. Cosmol. Astropart. Phys.* **09** (2011) 026.
- [14] F. M. White and J. Majdalani, *Viscous fluid flow*, 4th ed. (McGraw-Hill New York, 2022).
- [15] D. de las Heras, J. Renner, and M. Schmidt, Custom flow in overdamped Brownian dynamics, *Phys. Rev. E* **99**, 023306 (2019).
- [16] J. Renner, M. Schmidt, and D. de las Heras, Custom flow in molecular dynamics, *Phys. Rev. Research* **3**, 013281 (2021).
- [17] M. Schmidt and J. M. Brader, Power functional theory for brownian dynamics, *J. Chem. Phys.* **138**, 214101 (2013).
- [18] M. Schmidt, Power functional theory for Newtonian many-body dynamics, *J. Chem. Phys.* **148**, 044502 (2018).
- [19] D. de las Heras and M. Schmidt, Velocity Gradient Power Functional for Brownian Dynamics, *Phys. Rev. Lett.* **120**, 028001 (2018).
- [20] See Supplemental Material at <http://link.aps.org/supplemental/10.1103/PhysRevLett.128.094502> for details about simulations, custom flow, and power functional theory.
- [21] J. D. Weeks, D. Chandler, and H. C. Andersen, Role of repulsive forces in determining the equilibrium structure of simple liquids, *J. Chem. Phys.* **54**, 5237 (1971).
- [22] D. de las Heras and M. Schmidt, Flow and Structure in Nonequilibrium Brownian Many-Body Systems, *Phys. Rev. Lett.* **125**, 018001 (2020).
- [23] R. Kubo, The fluctuation-dissipation theorem, *Rep. Prog. Phys.* **29**, 255 (1966).
- [24] B. L. Holian, W. G. Hoover, B. Moran, and G. K. Straub, Shock-wave structure via nonequilibrium molecular dynamics and Navier-Stokes continuum mechanics, *Phys. Rev. A* **22**, 2798 (1980).
- [25] B. L. Holian, Modeling shock-wave deformation via molecular dynamics, *Phys. Rev. A* **37**, 2562 (1988).
- [26] E. Salomons and M. Mareschal, Usefulness of the Burnett Description of Strong Shock Waves, *Phys. Rev. Lett.* **69**, 269 (1992).
- [27] V. V. Zhakhovskii, S. V. Zybin, K. Nishihara, and S. I. Anisimov, Shock Wave Structure in Lennard-Jones Crystal via Molecular Dynamics, *Phys. Rev. Lett.* **83**, 1175 (1999).
- [28] M. Marciantie and M. S. Murillo, Thermodynamic and Kinetic Properties of Shocks in Two-Dimensional Yukawa Systems, *Phys. Rev. Lett.* **118**, 025001 (2017).
- [29] G. Falkovich, K. Gawędzki, and M. Vergassola, Particles and fields in fluid turbulence, *Rev. Mod. Phys.* **73**, 913 (2001).
- [30] L. Bentkamp, C. C. Lalescu, and M. Wilczek, Persistent accelerations disentangle Lagrangian turbulence, *Nat. Commun.* **10**, 3550 (2019).

- [31] S. Yamani, B. Keshavarz, Y. Raj, T.A. Zaki, G.H. McKinley, and I. Bischofberger, Spectral Universality of Elastoinertial Turbulence, *Phys. Rev. Lett.* **127**, 074501 (2021).
- [32] G. K. Vallis, *Atmospheric and Oceanic Fluid Dynamics* (Cambridge University Press, Cambridge, England, 2017).
- [33] G. R. Wang, F. Yang, and W. Zhao, There can be turbulence in microfluidics at low Reynolds number, *Lab Chip* **14**, 1452 (2014).
- [34] D. Di Carlo, Inertial microfluidics, *Lab Chip* **9**, 3038 (2009).
- [35] J. Zhang, S. Yan, D. Yuan, G. Alici, N.-T. Nguyen, M. Ebrahimi Warkiani, and W. Li, Fundamentals and applications of inertial microfluidics: A review, *Lab Chip* **16**, 10 (2016).
- [36] S. Roy, R. Raju, H.F. Chuang, B.A. Cruden, and M. Meyyappan, Modeling gas flow through microchannels and nanopores, *J. Appl. Phys.* **93**, 4870 (2003).
- [37] A. V. Straube, B. G. Kowalik, R. R. Netz, and F. Höfling, Rapid onset of molecular friction in liquids bridging between the atomistic and hydrodynamic pictures, *Commun. Phys.* **3**, 126 (2020).
- [38] N. Kavokine, R.R. Netz, and L. Bocquet, Fluids at the nanoscale: From continuum to subcontinuum transport, *Annu. Rev. Fluid Mech.* **53**, 377 (2021).
- [39] P. Coussot, *Mudflow Rheology and Dynamics* (Routledge, London, 2017). [10.1201/9780203746349](https://doi.org/10.1201/9780203746349)
- [40] M. P. Brenner, S. Hilgenfeldt, and D. Lohse, Single-bubble sonoluminescence, *Rev. Mod. Phys.* **74**, 425 (2002).
- [41] R. Toegel, S. Luther, and D. Lohse, Viscosity Destabilizes Sonoluminescing Bubbles, *Phys. Rev. Lett.* **96**, 114301 (2006).
- [42] M. Zakari and D. Jou, Equations of state and transport equations in viscous cosmological models, *Phys. Rev. D* **48**, 1597 (1993).
- [43] G. Jung, M. Hanke, and F. Schmid, Iterative reconstruction of memory kernels, *J. Chem. Theory Comput.* **13**, 2481 (2017).
- [44] H. Meyer, P. Pelagejcev, and T. Schilling, Non-Markovian out-of-equilibrium dynamics: A general numerical procedure to construct time-dependent memory kernels for coarse-grained observables, *Europhys. Lett.* **128**, 40001 (2020).
- [45] D. Lesnicki, R. Vuilleumier, A. Carof, and B. Rotenberg, Molecular Hydrodynamics from Memory Kernels, *Phys. Rev. Lett.* **116**, 147804 (2016).
- [46] J. O. Daldrop, B.G. Kowalik, and R.R. Netz, External Potential Modifies Friction of Molecular Solutes in Water, *Phys. Rev. X* **7**, 041065 (2017).